Nanotechnology

PAPER

Rolled-up single-layered vanadium oxide nanomembranes for microactuators with tunable active temperature

To cite this article: Xing Li *et al* 2019 *Nanotechnology* **30** 354003

Nanotechnology **30** (2019) 354003 (7pp) https://doi.org/10.1088/1361-6528/ab224d

Rolled-up single-layered vanadium oxide nanomembranes for microactuators with tunable active temperature

Xing Li[1,2], Yang Wang[2], Borui Xu[2], Xuefei Zhou[2], Chuanling Men[1], Ziao Tian[3] and Yongfeng Mei[2]

[1] School of Energy and Power Engineering, University of Shanghai for Science and Technology, Shanghai 200093, People's Republic of China
[2] Department of Materials Science, State Key Laboratory of ASIC and Systems, Fudan University, Shanghai, 200433, People's Republic of China
[3] State Key Laboratory of Functional Materials for Informatics, Shanghai Institute of Microsystem and Information Technology, Chinese Academy of Sciences, Shanghai 200050, People's Republic of China

E-mail: yfm@fudan.edu.cn

Received 24 February 2019, revised 29 April 2019
Accepted for publication 17 May 2019
Published 11 June 2019

Abstract

Multilayer vanadium dioxide (VO_2) actuators are a widespread concern as these micro/nano-actuators present a fast and efficient dynamic response when VO_2 occurs in metal–insulator transition (MIT) at 68 °C. By tuning the O_2 flow rate during oxide deposition and rolled-up nanotechnology, a microactuator based on a single-layered vanadium oxide nanomembrane with vertical component gradient is fabricated. Upward bending of the nanomembrane is driven by the release of the compressive strain gradient which is revealed through the difference in Raman shift of the vibration mode. Combining strain engineering, the initial curvature of microactuators is tuned in a wide range by the thickness of the nanomembranes. The actuation behavior from low curvature to high final curvature across the MIT is observed which depends on the nanomembrane thickness. Initial compressive strain distribution of the rolled-up nanomembrane decreases the MIT temperature simultaneously. Thus, taking advantage of the tunable MIT and reversible shape transformation, micro/nano-actuators with tunable triggering temperature, controllable initial curvature and large-displacement actuation are fabricated for curvature engineering in micromechanical systems.

Keywords: microactuator, vanadium dioxide, rolled-up nanotechnology, metal–insulator transition

(Some figures may appear in colour only in the online journal)

1. Introduction

Microactuators, transforming external stimuli to mechanical motion, have a wide range of applications including biomimetic robots [1], artificial muscle [2, 3], and microelectromechanical systems [4]. Fast response, large displacement, good flexibility, and low triggering threshold are most concerned in a microactuator. However, general microactuators are based on organic or organic/inorganic composite materials, which are difficult to meet these issues. For example, the response time of microactuators based on an ionic electroactive polymer or thermally active polymer is more than 0.1 s, and triggering threshold is over 1 kV or 200 °C that limited the range of applications [5, 6]. Therefore, a material with low triggering temperature, below milliseconds of response time and easy to fabrication is desired to be designed for microactuators.

Vanadium dioxide (VO_2) is a strongly correlated electronic material with intriguing metal–insulator transition (MIT). The triggering temperature of VO_2 is 68 °C and response time can reach 10 ms. The phase transition of VO_2 generates 1%–2% compressive strain during transition process from insulator phase to metal phase which can serve as microactuators [7] to be applied in micro/nano-electromechanical systems [8], microrobotics [9] and biomimetics [10, 11]. Recently, various microactuators have been investigated based on bilayer structures. These microactuators were generally constructed by depositing a structural layer on a VO_2 film, followed by an etching process to define the anchor and pattern [12]. The initial state of these microactuators was altered by the deposited materials with tunable properties and internal strain [13]. Unfortunately, the active layer in these microactuators can only be set as the bottom layer. Moreover, deposition of VO_2 requires a high temperature [7–13], which means few materials of underlayer materials with VO_2 can be chosen as strain layer for a VO_2 microactuator. So the shrinking of the VO_2 layer results in downward bending during actuation or unfolding behavior to a bended microactuator. These limitations hamper the potential of VO_2-based microactuators to be applied in a general situation, especially in an on-chip system in which a downward bending is not allowed. Moreover, the introduction of external materials will cause unexpected side effects [8, 14–16].

Rolled-up nanotechnology, through which 3D microstructures are fabricated by strain engineering in 2D patterned nanomembranes, have proved their capability among on-chip opto-electronics [17, 18] and off-chip micromachines [19, 20]. Benefiting from the compatibility and designability in materials and structures, primary demonstrations on microactuators constructed by rolled-up nanotechnology have been demonstrated with stimuli-responsive materials [21, 22]. Here, we fabricated a single-layered vanadium oxide nanomembrane consisting of VO_x and VO_2 hierarchical components by tuning the oxygen flow rate during deposition. The hierarchical components generate an internal strain gradient, leading to the rolling of the single-layered nanomembrane after the etching of sacrificial underlayer. The diameter of the curved nanomembrane can be manipulated by altering the thickness, which provides capability in structure design of microactuators. The actuation behavior in which the nanomembrane rolled upwards into a tighter state was established on the shrinking of upper VO_2 component due to its MIT triggered by heat. Furthermore, the active temperature is tuned by the redistribution of compressive strain inside VO_2 that the temperature decreases with rising initial curvature. This work proposed a VO_2-based microactuator with a simple one-step deposition process. This designable microactuator with tunable active temperature would provide great potential in phase transition-based electronics, photonics and micromechanics.

2. Experimental detail

2.1. Growth and characterization of vanadium oxide nanomembranes

Firstly, SiO_2 coated Si substrate was cleaned by ultrasonication in acetone, ethanol and deionized water for 5 min. After cleaning, VO_x component was grown on SiO_2/Si substrates by direct-current magnetron sputtering at 300 °C. The growth pressure, Ar/O_2 gas flow, and deposition time were 10.41 mTorr, 55/45 sccm, and 4 min, respectively. Afterwards, the temperature was increased to 500 °C to deposit VO_2 component on VO_x. Ar/O_2 gas flow is 60/40 sccm. The pressure is 11.18 mTorr, and growth time is 30 min. The structure of nanomembrane was characterized by x-ray diffraction (XRD). The angle of incidence was fixed at 0.6°, and the measurement was taken using a 2θ scan geometry. The nanomembrane was also characterized by micro-Raman scattering spectroscopy (Horiba JY HR-800) with 514 nm Ar laser and transmission electron microscopy (TEM, FEI TECNAI G2 S-TWIN F20). Before the characterization by TEM, the sample preparation was conducted via focused ion beam (FIB, FEI Helios NanoLab 600). The electrical properties of nanomembrane were measured using a Keithley 4200 semiconductor characterization system.

2.2. Fabrication of single-layered vanadium oxide microactuators

In the first step, thinning of vanadium oxide nanomembrane was realized by reactive ion etching (RIE) with 10 sccm CF_4 flow rate, 30 sccm Ar flow rate, 300 mTorr chamber pressure, and 100 W power. Vanadium oxide nanomembranes with various thicknesses of 20, 25, and 35 nm, were fabricated by altering the etching time from 15 to 7 s. Then, a layer of photoresist (AZ-5214, Micro-chemicals GmbH, Germany) with about 1 μm thickness was spin-coated and etching windows were patterned by photolithography. Thirdly, exposed part of the sample was etched by RIE for 30 s in same condition as described above. After that, patterned nanomembrane was released from the substrate by selectively etching SiO_2 sacrificial layer using 40% HF (hydrofluoric acid) solution at room temperature. Finally, critical point drying (CPD030 Critical Point Dryer from Bal-Tec AG) was applied to dry the rolled-up single-layered vanadium oxide microactuators without structural collapse.

2.3. Characterization of single-layered vanadium oxide microactuators

The morphological properties of single-layered vanadium oxide microactuators were characterized via scanning electron microscopy (SEM, JEOL JSM-6701F). Additionally, micro-Raman scattering spectroscopy (Horiba JY HR-800) with 514 nm Ar laser was utilized to analyze the strain distribution in microactuators with different initial diameters. Eventually, the actuation ability of the microactuators was triggered by heating and cooling, and recorded by an optical microscopy with CCD camera.

3. Results and discussion

The TEM image in figure 1(a) presents the hierarchical components consisting of VO_2 and VO_x in the single-layered vanadium oxide nanomembrane. There is a clear boundary

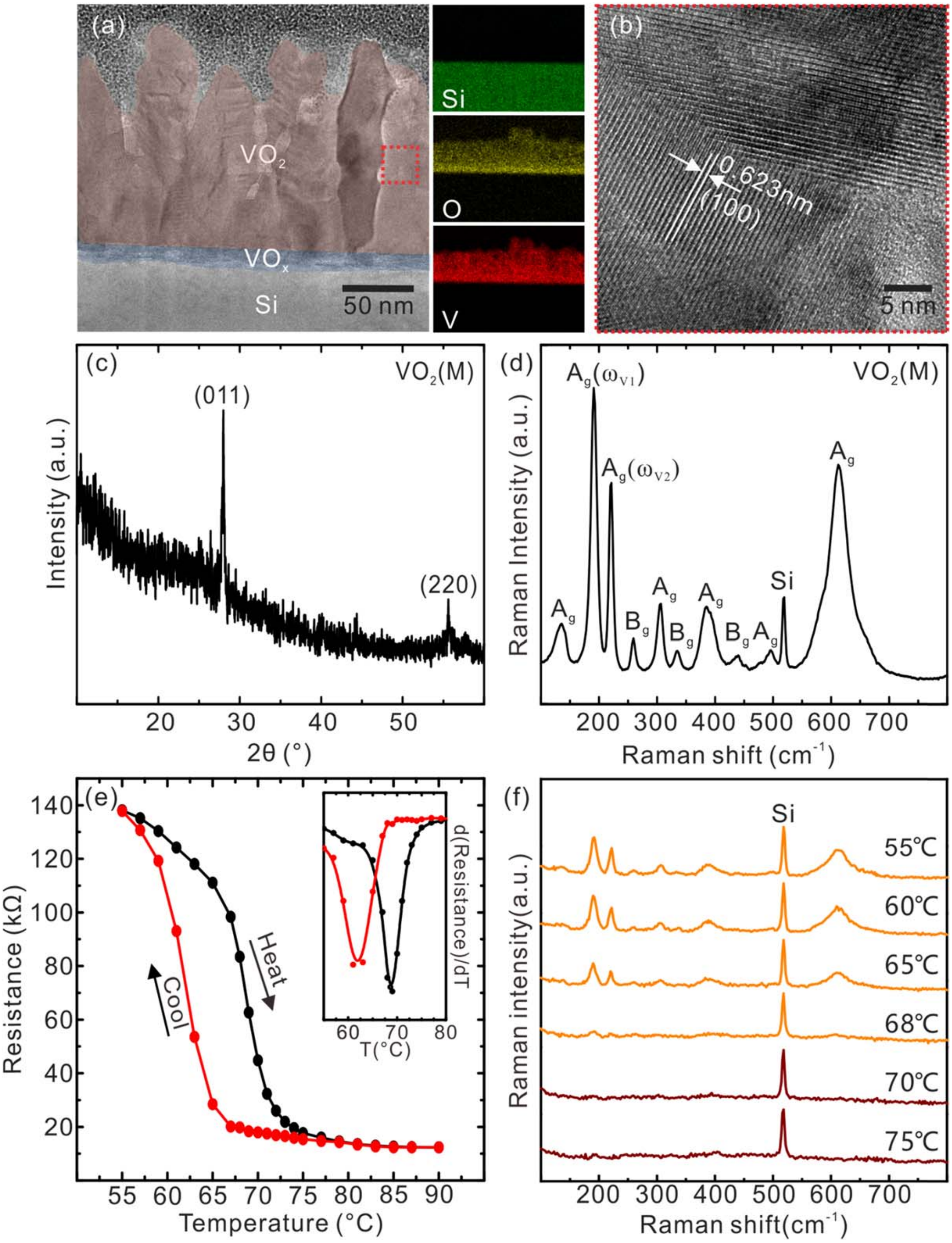

Figure 1. Characteristics and MIT of single-layered vanadium oxide nanomembrane with hierarchical components. (a) TEM image from the cross section of vanadium oxide nanomembrane and corresponding elemental mapping of silicon, oxygen and vanadium, respectively. (b) High-resolution TEM image of the VO_2 component in the nanomembrane. (c) X-ray diffraction pattern of the VO_2 component. (d) Raman spectrum of VO_2 component. (e) Temperature-dependent resistance of the VO_2 component with MIT. The inset is corresponding differential resistance related to temperature. (f) Raman spectrum of vanadium oxide nanomembrane evolving with temperature.

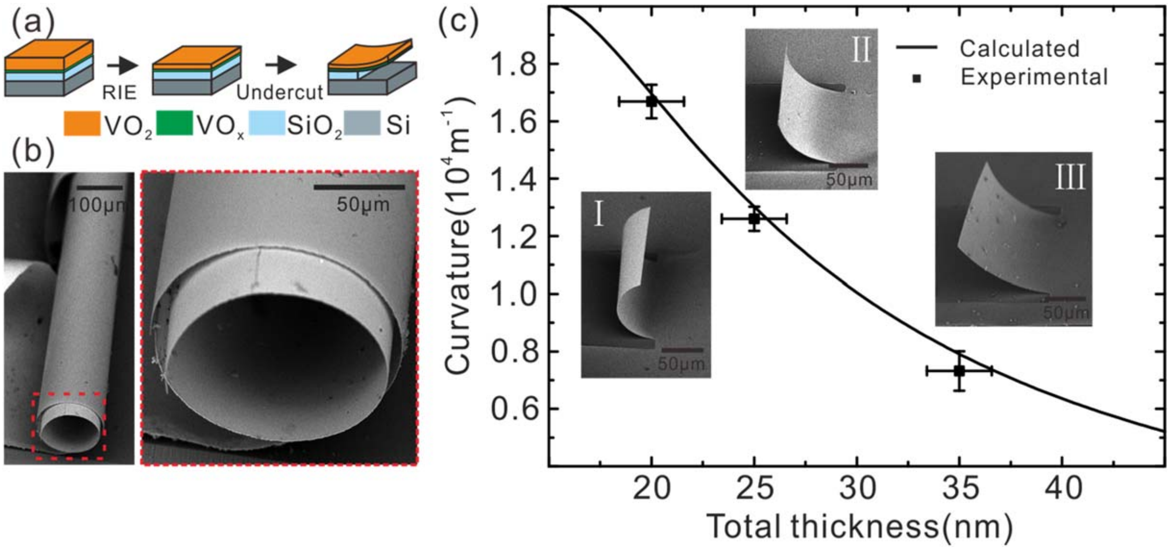

Figure 2. Rolling of single-layered vanadium oxide nanomembrane. (a) The schematic of the fabrication process using rolled-up nanotechnology. (b) SEM image of rolled-up microtube at low (left) and high magnification (right). (c) Summary of rolled-up vanadium oxide nanomembrane curvature as a function of vanadium oxide nanomembrane thicknesses and corresponding SEM images. The solid line represents the calculated curvature described by equation (1).

between these two components, where textured polycrystalline VO_2 with 160 nm is shown in upper part and amorphous VO_x with 10 nm is shown in lower part. The elemental compositions of Si, O and V were evidenced by the energy-dispersive x-ray elemental mapping as shown in right panels of figure 1(a). It is clearly observed that, compared to the VO_2 component, the VO_x component grown by magnetron sputtering with higher oxygen flow rate contains a higher ratio of oxygen. High crystal quality of VO_2 part was observed in high-resolution TEM image as shown in figure 1(b) and the lattice spacing of 0.623 nm is corresponding to the (100) plane. XRD pattern of polycrystalline VO_2 is shown in figure 1(c). Two peaks near 27.98° and 55.65° are attributed to (011) and (220) planes of VO_2, respectively. In figure 1(d), Raman spectrum taken with 514 nm laser excitation displays a set of peaks ranging from 137 to 612 cm^{-1}, confirming the existence of standard monoclinic insulating phase of VO_2. Here, the A_g and B_g are two Raman modes which are Raman vibrations in the low-temperature M phase of VO_2 [23]. Besides, two low-frequency phonons ω_{V1} (189.0 cm^{-1}) and ω_{V2} (218.9 cm^{-1}) correspond to V–V lattice motion, and other Raman peaks are attributed to V–O vibration modes [24, 25]. To test the MIT of the upper VO_2 component in the single-layered vanadium oxide nanomembrane, electrical resistance related to temperature was measured in figure 1(e). A dramatic decrease in resistance with increasing temperature was obtained, elucidating successful MIT through the nanomembrane. A derivative analysis on resistance was applied as shown in the inset of figure 1(e) to define the MIT temperature and transition slope temperature, that is, the center of the peak is the MIT temperature and the full width at half maximum is the transition slope temperature. Hence, MIT temperature and transition slope temperature are 68.76 °C and 6.83 °C, respectively. The MIT was further clarified through Raman spectrum as present in figure 1(f). All modes of M phase decrease with increasing temperature. When the temperature rises to the phase transition point, all Raman peaks of VO_2 disappear owing to the complete transformation of M phase into metallic R phase. Phase transition temperature obtained by Raman is in agreement with the one obtained by electrical resistance examination. These results indicate the successful fabrication of single-layered vanadium oxide nanomembrane with hierarchical components through controlling parameters in the process of magnetron sputtering. And MIT of this nanomembrane is established in the upper VO_2 component of which the temperature was kept at 68 °C as is in initial VO_2.

For the hierarchical component vanadium oxide nanomembrane, different oxygen ratio between VO_2 and VO_x component generates strain gradient in the nanomembrane for rolling into microactuators with different diameters. Figure 2(a) shows the schematic of microfabrication process as aforementioned. Driven by strain gradient, free-standing vanadium oxide nanomembrane bent into a microtube as shown in figure 2(b). To construct a rolled-up microactuator rather than a microtube, the length of released vanadium oxide was decreased. Figure 2(c) shows the average curvature of single-layered vanadium oxide microactuators. The microactuators I, II and III are rolled-up from vanadium oxide nanomembrane of which the thickness is tuned as 20, 25 and 35 nm while the thickness of VO_x keeps 10 nm. It is observed that the curvature decreases with rising thickness. To quantitatively describe the curvature variation as a function of strain and nanomembrane thickness, we refer the linear strain theory model used for bilayer systems [26]. According to this theory model, we divide the nanomembrane into two regions. The VO_x component is a relaxed layer which is close to the interface of the deposited layer/sacrificial layer, as well as the upper VO_2 region is a strained layer. We assume that the elastic coefficients are equal in the two regions. The curvature

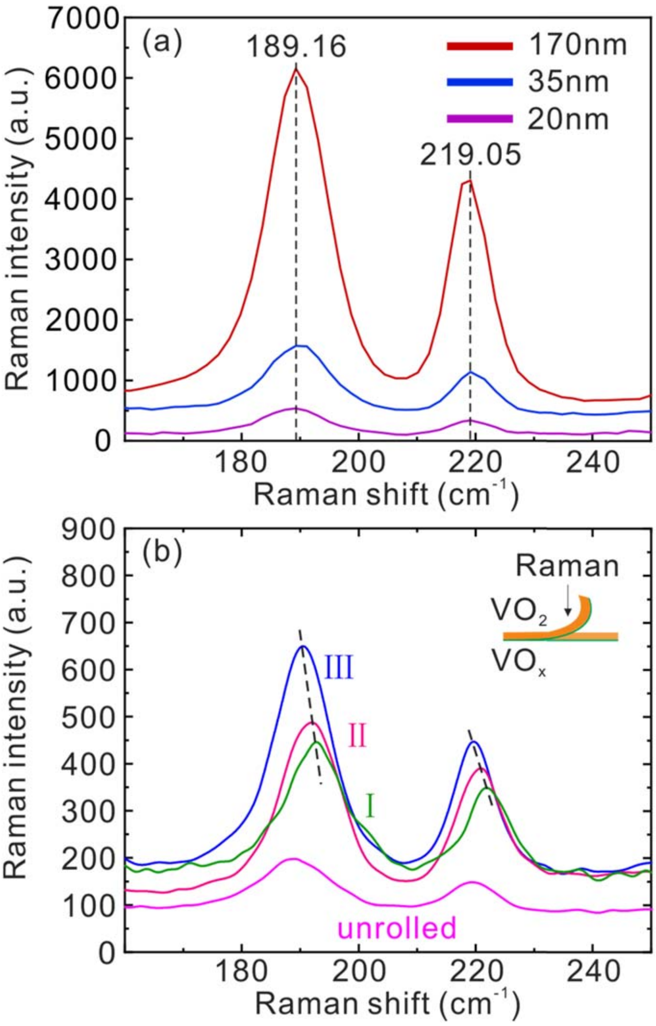

Figure 3. (a) Raman spectra of single-layered vanadium oxide nanomembrane with different thickness before release. (b) Raman spectra of rolled-up single-layered vanadium oxide nanomembrane with different thickness (I: 20 nm, II: 25 nm and III: 35 nm). The inset shows schematic of rolled-up nanomembrane under illumination of a laser beam to measure the Raman signal in VO_2 component.

K of rolled-up microstructure can be calculated by [26]

$$K = \frac{6\varepsilon(1+v)d_{\text{strain}}d_{\text{relax}}}{(d_{\text{strain}}+d_{\text{relax}})^3}, \quad (1)$$

where $\varepsilon = 0.0174\%$ is the strain in VO_2 component of unrolled nanomembrane calculated by Raman frequency shift in the figure 3(a) and the v is the Poisson ratio (0.3) [27]. VO_x component d_{relax} is kept in constant as 10 nm and the thickness of VO_2 component d_{strain} ranges from 10 to 25 nm. The solid line of calculated curvature in figure 2(c) indicates that the model agrees well with the experimental results.

To clarify the strain distribution in rolled-up nanomembrane, figure 3(b) shows the Raman spectra for rolled-up microstructures with various curvature. As the laser illuminated the upper surface of single-layered vanadium oxide nanomembrane, the excited signal mainly generated from VO_2 component. The peak position at 189 and 219 cm^{-1} is attributed to the low-frequency phonons (ω_{V1} and ω_{V2}) of V–V lattice motion, which is calculated by isotope substitution and density functional theory [28].

The ω_{V1} and ω_{V2} phonons, with more significant Raman modes shifts, possess higher sensitivity to strain variation than other phonons [29]. The Raman signal of low-frequency phonons (ω_{V1} and ω_{V2}) collected from microactuators shows associated intensity increase and a slight spectral shift comparing to the unrolled vanadium oxide nanomembrane. Simultaneously, Raman intensity is a positive correlation to the thickness of vanadium oxide nanomembrane in microactuators, and the intensity of the rolled-up nanomembrane is higher than the one of unrolled nanomembrane.

With increasing thickness of microactuators from I to III and unrolled nanomembrane, the ω_{V1} phonon presents a redshift from 192.84 to 189.16 cm^{-1} and the redshift of ω_{V2} phonon is from 221.56 to 219.05 cm^{-1}. These shifts of ω_{V1} and ω_{V2} phonons caused by compressive strain can be determined by [30]

$$\Delta\omega_{\text{alloy}} = \frac{1}{2\omega_0}(p+2q)\cdot\varepsilon, \quad (2)$$

where ε is the strain distribution in VO_2, ω_0 refers to original ω_{V1} (189 cm^{-1}) and ω_{V2} (218.96 cm^{-1}) of unstrained VO_2. The p and q are linear interpolations between the value of V–V that are extrapolated from [29]. In our case, $(p+2q)_{\omega_{V1}}$ is equal to $3.49\times10^5 \pm 0.15\times10^5$ s^{-2} and $(p+2q)_{\omega_{V2}}$ is equal to $2.49\times10^5 \pm 0.18\times10^5$ s^{-2}. The strain of microactuators I, II and III were calculated by shift of ω_{V1} (ω_{V2}) phonon as 0.42% (0.45%), 0.32% (0.31%), and 0.16% (0.12%), respectively.

As aforementioned, the phase transition of VO_2 will generate 1%–2% compressive strain during the transition which supplies the possibility to make VO_2 as a heat-driven microactuator. Figure 4(a) presents the actuating behavior of the microactuator II in a heating-cooling cycle. The dark part is the microactuator, whose area decreases with increasing temperature, reflecting an upward bending of microactuator. The actuation behavior from small to large final curvature owes to the phase transition of VO_2, leading to additional compressive strain in upper part of microactuator. Then the system starts to cool to room temperature. VO_2 suffers from an opposite transition so that the microactuator returns to initial curvature. Thus, the curvature increases in heating and reduces in cooling, opposite to reported microactuators in which VO_2 serves as the bottom layer. The variation in curvature of microactuators I, II and III during heating and cooling are present in figure 4(b). As the initial curvature is different with the thickness of nanomembrane as discussed in figure 2(c), we normalized the initial curvature of microactuator with different nanomembrane thickness to comfortably compare their curvature changes during the phase transition. The great change in curvature is attributed to the low bending stiffness of ultra-thin vanadium oxide nanomembrane, leading to lower requirement of actuating energy. Besides, it represents that with reduction of the vanadium oxide nanomembrane thickness, the range of curvature changes during actuation is wider, which owes to the decreasing bending stiffness in thinner nanomembrane. Here,

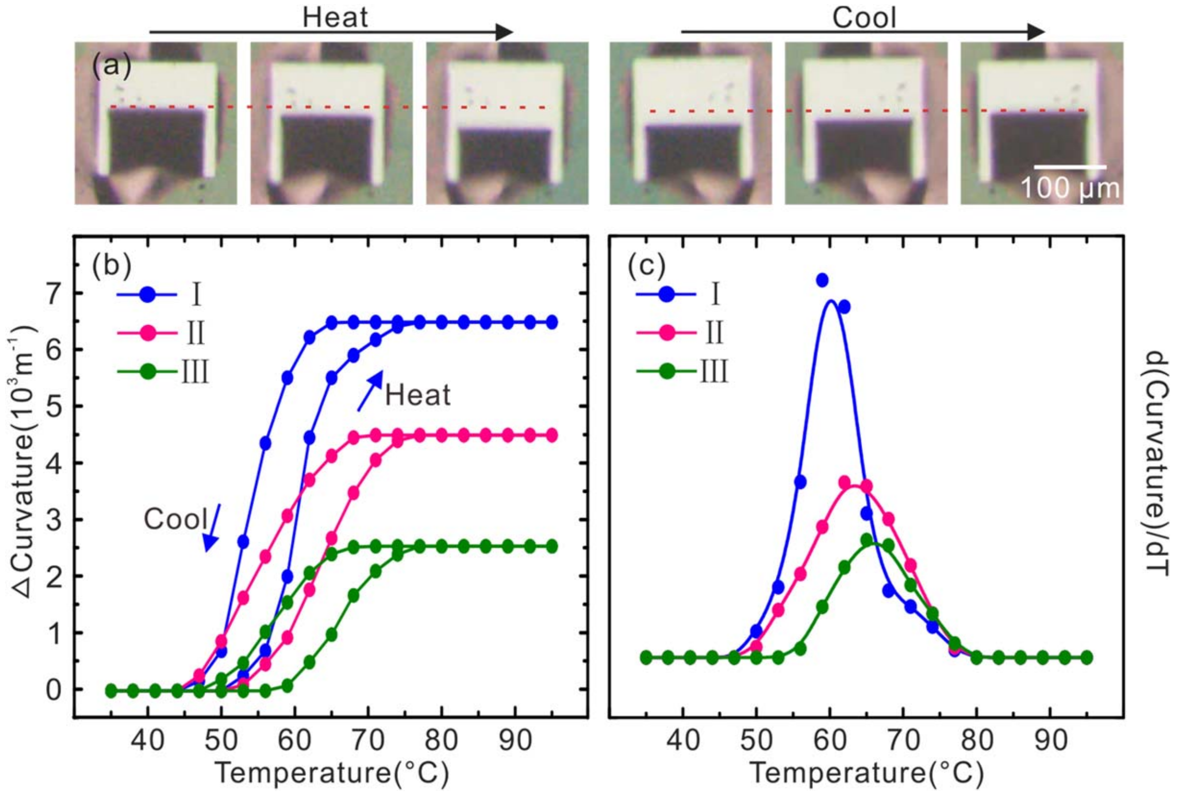

Figure 4. Properties of rolled-up single-layered vanadium oxide microactuator responsive to temperature. (a) Optical images of microactuator II in a heating-cooling cycle. (b) Variation in curvature of microactuators in a heating-cooling cycle. (c) Corresponding differential curvature related to temperature.

the capability of these microactuators can be describe by volumetric work density which is given by $E \times \Delta\varepsilon^2/2$, where E is the Young's modulus of the VO_2 (~140 GPa) and the $\Delta\varepsilon$ is calculated by equation (1). The maximum work density was estimated to reach 0.031 J cm^{-3}, which is much higher than human muscle (~0.008 J cm^{-3}) [3]. Moreover, figure 4(c) shows differential analysis of curvature, reflecting that the temperature of phase transition moves to lower area in thinner microactuators. This variation is considered as a consequence of compressive strain redistribution in rolled-up microactuators. The phase transition temperature turns to 60.19 °C in microactuator I corresponding to 0.43% strain calculated by Raman spectrum. With different thickness of single-layered vanadium oxide microactuator, the MIT temperature can be tuned by different strain states.

4. Conclusion

In summary, we demonstrated a novel and simple approach to fabricate a tunable single-layered vanadium oxide microactuator based on rolled-up nanotechnology. Different layer components in the microactuator were deposited by controlling the oxygen flow rate in magnetron sputtering which generate a strain gradient to drive the nanomembrane bending upwards. The thickness controlled by further thinning process of the nanomembrane offers tunability in initial curvature of rolled-up nanomembrane. Benefiting from MIT in upper VO_2 component, the single-layered vanadium oxide nanomembrane suffers a great curvature increase into a tighter rolling state with heat stimulus. As the initial curvature decreases in the thinner nanomembrane, compressive strain redistribution in the VO_2 layer component increases leading to a lower MIT temperature, so that the actuation behavior can be controlled by the fabrication process. When the nanomembrane thickness decreases from 35 to 20 nm, the MIT temperature of the microactuator decreases from 68.71 °C to 60.19 °C with enhanced curvature change. Such microactuator driven by MIT requires a small quantity of actuation energy with a rapid response to heating or cooling. Such microactuators with controllable initial curvature, large-displacement actuation, controllable phase transition temperature and simple fabrication method could envision a wide range of micro- and nanoscale applications such as micromanipulation, optomechanical and electromechanical switch, microfluidic valving and pumping, drug delivery, heat regulation, and artificial muscle.

Acknowledgments

This work is supported by the National Natural Science Foundation of China (U1632115, 51711540298), Science and Technology Commission of Shanghai Municipality (17JC1401700), the Changjiang Young Scholars Program of China and the Program of Shanghai Academic Research

Leader (19XD1400600). Part of the experimental work has been carried out in Fudan Nanofabrication Laboratory and Shanghai Institute of Microsystem and Information Technology.

ORCID iDs

Yongfeng Mei https://orcid.org/0000-0002-3314-6108

References

[1] Chen P, Xu Y, He S, Sun X, Pan S, Deng J, Chen D and Peng H 2015 Hierarchically arranged helical fibre actuators driven by solvents and vapours *Nat. Nanotechnol.* **10** 1077–83
[2] Lima M D *et al* 2012 Electrically, chemically, and photonically powered torsional and tensile actuation of hybrid carbon nanotube yarn muscles *Science* **338** 928–32
[3] Mirfakhrai T, Madden J D W and Baughman R H 2007 Polymer artificial muscles *Mater. Today* **10** 30–8
[4] Snyder G J, Lim J R, Huang C K and Fleurial J P 2003 Thermoelectric microdevice fabricated by a mems-like electrochemical process *Nat. Mater.* **2** 528–31
[5] Huu Chuc N, Thuy D V, Park J, Kim D, Koo J, Lee Y, Nam J D and Choi H R 2008 A dielectric elastomer actuator with self-sensing capability *Proc. SPIE* **6927** 69270V
[6] Yuan W *et al* 2008 Fault-tolerant dielectric elastomer actuators using single-walled carbon nanotube electrodes *Adv. Mater.* **20** 621–5
[7] Dong K *et al* 2018 A 0.2 V micro-electromechanical switch enabled by a phase transition *Small* **14** 1703621
[8] Liu K, Cheng C, Cheng Z, Wang K, Ramesh R and Wu J 2012 Giant-amplitude, high-work density microactuators with phase transition activated nanolayer bimorphs *Nano Lett.* **12** 6302–8
[9] Shahinpoor M 2003 Ionic polymer-conductor composites as biomimetic sensors, robotic actuators and artificial muscles-a review *Electrochim. Acta* **48** 2343–53
[10] Ma H, Hou J, Wang X, Zhang J, Yuan Z, Xiao L, Wei Y, Fan S, Jiang K and Liu K 2016 Flexible, all-inorganic actuators based on vanadium dioxide and carbon nanotube bimorphs *Nano Lett.* **17** 421–8
[11] Cao J, Fan W, Zhou Q, Sheu E, Liu A, Barrett C and Wu J 2010 Colossal thermal-mechanical actuation via phase transition in single-crystal VO_2 microcantilevers *Appl. Phys. Lett.* **108** 083538
[12] Zhang J, Torres D, Ebel J L, Sepulveda N and Tan X 2016 A composite hysteresis model in self-sensing feedback control of fully integrated VO_2 microactuators *IEEE/ASME Trans. Mechatronics* **21** 2405–17
[13] Dong K, Lou S, Choe H S, Liu K, You Z, Yao J and Wu J 2016 Stress compensation for arbitrary curvature control in vanadium dioxide phase transition actuators *Appl. Phys. Lett.* **109** 023504
[14] Liu K, Cheng C, Suh J, Tang-Kong R, Fu D, Lee S, Zhou J, Chua L O and Wu J 2013 Powerful, multifunctional torsional micromuscles activated by phase transition *Adv. Mater.* **26** 1746
[15] Ou J Y, Plum E, Zhang J and Zheludev N I 2013 An electromechanically reconfigurable plasmonic metamaterial operating in the near-infrared *Nat. Nanotechnol.* **8** 252–5
[16] Ou J Y, Plum E, Jiang L and Zheludev N I 2011 Reconfigurable photonic metamaterials *Nano Lett.* **5** 2142–4
[17] Huang G, Kiravittaya S, Bolanos Q V A, Ding F, Benyoucef M, Rastelli A, Mei Y and Schmidt O G 2009 Optical properties of rolled-up tubular microcavities from shaped nanomembranes *Appl. Phys. Lett.* **94** 141901
[18] Ji H X, Wu X L, Fan L Z, Krien C, Fiering I, Guo Y G, Mei Y and Schmidt O G 2010 Self-wound composite nanomembranes as electrode materials for lithium ion batteries *Adv. Mater.* **22** 4591–5
[19] Ning H, Zhang Y, Zhu H, Ingham A, Huang G, Mei Y and Solovev A A 2018 Geometry design, principles and assembly of micromotors *Micromachines* **9** 75
[20] Xu B, Zhang B, Wang L, Huang G and Mei Y 2018 Tubular micro/nanomachines: from the basics to recent advances *Adv. Funct. Mater.* **28** 1705872
[21] Xu B, Tian Z, Wang J, Han H, Lee T and Mei Y 2018 Stimuli-responsive and on-chip nanomembrane micro-rolls for enhanced macroscopic visual hydrogen detection *Sci. Adv.* **4** 8203
[22] Tian Z, Xu B, Hsu B, Stan L, Yang Z and Mei Y 2018 Reconfigurable vanadium dioxide nanomembranes and microtubes with controllable phase transition temperatures *Nano Lett.* **18** 3017–23
[23] Schilbe P 2002 Raman scattering in VO_2 *Physica* B **316** 600–2
[24] Srivastava R and Chase L L 1971 Raman spectrum of semiconducting and metallic VO_2 *Phys. Rev. Lett.* **27** 727–30
[25] Petrov G I, Yakovlev V V and Squier J 2002 Raman microscopy analysis of phase transformation mechanisms in vanadium dioxide *Appl. Phys. Lett.* **81** 1023–5
[26] Songmuang R, Deneke C and Schmidt O G 2006 Rolled-up micro- and nanotubes from single-material thin films *Appl. Phys. Lett.* **89** 223109
[27] Fan W *et al* 2011 Large kinetic asymmetry in the metal-insulator transition nucleated at localized and extended defects *Phys. Rev.* B **83** 235102
[28] Marini C *et al* 2008 Optical properties of $V_{1-x}Cr_xO_2$ compounds under high pressure *Phys. Rev.* B **77** 235111
[29] Atkin J M, Berweger S, Chavez E K, Raschke M B, Cao J, Fan W and Wu J 2012 Strain and temperature dependence of the insulating phases of VO_2 near the metal-insulator transition *Phys. Rev.* B **85** 020101
[30] Songmuang R, Jinphillipp N Y, Mendach S and Schmidt O G 2006 Single rolled-up SiGe/Si microtubes: structure and thermal stability *Appl. Phys. Lett.* **88** 021913